A. Airoldi, N. Novak, F. Sgobba, A. Gilardelli, M. Borovinšek
Foam-Filled Energy Absorbers with Auxetic Behaviour for Localized Impacts
Materials Science and Engineering A: Structural Materials: Properties, Microstructures and Processing, In press - Published online 07/05/2020
doi:10.1016/j.msea.2020.139500

Foam-filled energy absorbers with auxetic behavior for localized impacts

A. Airoldi[1], N. Novak[2], F. Sgobba[1], A. Gilardelli[1], M. Borovinšek[2]

*[1]*Department of Aerospace Science and Technology, Politecnico di Milano, Milano, Italy*

[2]*Faculty of Mechanical Engineering, University of Maribor, Maribor, Slovenia*

Emails: alessandro.airoldi@polimi.it , francesco.sgobba@mail.polimi.it, n.novak@um.si , matej.borovinsek@um.si

Abstract

The paper proposes an innovative concept for energy absorption in case of localized impacts. The concept is based on the contraction capability of cellular structures with negative Poisson's ratio under impact, which is combined with the energy absorption capability of a foam filler. An experimental assessment was accomplished considering a 3D-printed polymeric hexa-chiral frame filled with open-cell soft polyurethane foam inserts, subjected to quasi-static and dynamic indentation. The energy absorbed by the combination of the auxetic frame and foam is significantly higher than the sum of the energies absorbed by constituent elements tested separately. Based on the experiments, a numerical approach for foam-filled absorbers is developed and validated. Then non-linear models of metallic chiral units are considered in a genetic optimization process, set up to optimize the maximum frame contraction under compression before its failure. Finally, the previously validated numerical approach is applied to the optimised geometries, and it is shown that the foam filler can provide significant enhancement of specific absorbed energy and load uniformity ratio also for frames made of ductile metallic material.

Keywords: energy absorption, chiral honeycomb, auxetic materials, optimization, localized impacts

1. Introduction

The progress in science and technology enables engineers to produce more advanced composite materials, which offer safer and more efficient transportation, buildings, clothes and other engineering parts [1]. In the last decades, composite sandwich panels with core from cellular materials are in use especially for crash absorption, blast and ballistic protection, thermal and sound insulation [1]. A common configuration is based on low stiffness material entrapped between two solid plates: the outer skin provides load carrying capability while the inner core provides energy absorption capabilities. Usually the core of sandwich panels is made of a cellular structure, with smaller or larger pores. Such pores can also be filled with other types of material, thus enabling a hierarchical energy absorption on different length scales with a potential benefit in greater energy absorption capabilities. Energy absorbers with such characteristics are promising composite structures and meta-materials that could provide superior mechanical properties compared to conventional materials.

Composite sandwich tubes made from glass fibres, polystyrene foam and epoxy resin with tubular inserts were tested under quasi-static compression in [2], where also the effect of design variables and their interactions were studied. Lateral crushing of polyurethane foam-filled epoxy composite tubes made from natural flax fabric composite was evaluated in [3]. The influence of design parameters (tube thickness, inner diameter and foam filler) on the mechanical response was evaluated, where the main conclusion was that filled composite tubes are able to spread the deformation under lateral loading and enhance energy absorption. It also was found that the specific energy of the empty and foam-filled flax/epoxy tubes in lateral crushing were significantly lower than those in axial crushing [3]. Axial crush performance of

aluminium tubes filled with hybrid foam (aluminium foam and polymer [4]) was evaluated in [5], where it was shown that the increase in specific energy absorption can be up to 78 % higher in comparison to the empty tubes. Furthermore, the aluminium tubes were also filled with closed-cell foam [6] and foam with advanced pore morphology [7]. Filling with closed-cell foams was also investigated considering in-situ techniques, where the aluminium foam was fabricated inside the tube, thus achieving a stronger interface between the tube and foam [8,9]. Foam-filled tubes with transversely graded foam and wall thickness were evaluated and optimised in [10], where combination of experiments and computational simulations were used. It was found that the functionally graded crush absorber with an ascending transverse foam density could largely improve the specific energy absorption and only slightly increase the maximum force. The study on energy absorption of curved plate filled with aluminium foam is given in [11,12]. The actual application as a blast resistant building was studied and it was proved that filling the structure with aluminium foam enhances blast resistance. Polyvinyl chloride foam-filled aluminium honeycombs were evaluated with homogenisation technique in [13], where it was proven, that foam filling leads to enhance in- and out- of plane properties of honeycombs. Low-speed impact of a sandwich panel with a filled honeycomb core was studied in [14]. The results show that the filled sandwich panel provides superior impact resistance capacity in comparison with the hollow honeycomb panel.

Auxetic materials and meta-materials are a relatively new class of materials [15,16], which possess negative Poisson's ratio and therefore offer some enhancements in mechanical behaviour which can also improve behaviour of crash absorbers [17,18]. Special group of auxetic materials are chiral auxetic structures [19], which's mechanical behaviour was evaluated under axial compression loading [20] and impact loading [21,22]. Auxetic materials can be a part of crash absorber as a crushable core, or also as a filler material of a sandwich

panel's core. Most of experimental tests and computational studies of absorbers with auxetic behaviour are for now done under uniaxial quasi-static and dynamic regime [23–26] and some limited research was done in the field of high strain rate loading behaviour [27–30]. Several types of cellular structures exhibit auxetic response. For instance, in-plane elasticity of a novel auxetic honeycomb with a combination of re-entrant hexagonal geometry and thin plane was evaluated in [31]. The theoretical and numerical models for tensile modulus, shear modulus and Poisson's ratio were developed and showed good agreement with experiments. Such type of cellular topologies can be used to enhance energy absorption capabilities, exploiting the auxetic effect that densifies material under compressive loading. Blast response study of sandwich structures with graded and non-graded auxetic cores was evaluated in case of re-entrant [29,32] and chiral [33] geometry, where it was proven that the auxetic core can enhance the response under blast loading. Negative Poisson's ratio is also exhibited by foams and square tubes filled with polymeric auxetic foam, which were analysed under quasi-static [34] and dynamic [35] loading. It was determined that increasing the auxeticity level of a foam filler enhances crashworthiness of foam-filled structures under both quasi-static and dynamic loading conditions. Auxetic lay-up of composite laminates can be also conceived by using standard unidirectional plies. Low-velocity impact response of multilayered structural composites with auxetic effect was studied in [36]. It was concluded that the auxetic composite has a better energy absorption performance. The application of auxetic springs filled with foam in composite seats was studied in [37]. It was shown that filled and non-filled seats exhibited comparable stiffness and comfort.

As can be seen from the above review, the work done on the field of auxetic energy absorbers filled with foam is quite limited. Especially, there are no studies on the field of localised impact on foam-filled auxetic crash absorbers despite auxetic effects could provide significant

improvements in the impact response and specific energy absorption levels. From these reasons, it follows a need for the development of a concept of novel crash absorber with optimised auxetic frame filled with foam, which will lead to possible enhancement of energy absorption capabilities for novel crash absorbers subjected to localized impacts. In the concept presented in this paper, auxeticity is provided by a frame with a periodic chiral topology, which is filled with a commercially available energy absorbing foam having a non-auxetic response. Experiments are conducted considering a polymeric 3D printed frame, filled by open-cell polyurethane foam, as presented in the second section of the papers, following this introduction. A numerical approach is developed and validated in the third section. Thereafter, an optimization of the frame properties is conducted in the fourth section, considering a metallic material, and the performances of a new absorber configuration is studied by applying the validated numerical approach. The findings of the research activities are summarized in the final section.

2. Experiments on foam-filled polymeric chiral frames subjected to indentation

2.1 Design and manufacturing of the energy absorbers

A first experimental evaluation of the concept proposed in this paper was based on a 3D printed polymeric chiral frame filled by a visco-elastic foam subjected to a local indentation at two different velocities. The absorbers consisted of a rectangular element, with a length of 193 mm, a height of 93 mm and a depth of 25 mm. Three types of absorbing elements were tested: a pure foam element, an element made of a polymeric chiral frame, and the frame filled by pre-cut inserts of foam. Tests were performed with a MTS 858 Minibionix II system, with an impactor represented by a steel cylinder with a diameter of 100 mm. An indentation at a constant velocity

of 1 mm/s was performed to evaluate the response in a static indentation, whereas a dynamic indentation test was performed at a constant velocity of 500 m/s. In all the tests the impacting surface of the element was reinforced by a sheet of Al6060 alloy with a thickness of 0.5 mm, bonded to the upper surfaces of the absorbers. Such plate was mainly used to avoid local failures of the impacting surface of the two absorbers with the polymeric frame, but was also used in the pure foam absorber to obtain the same impacting conditions.

The filler material chosen was a CF-45M foam, with a density of 96 kg/m^3, which is one of the commercially available versions of Confor® open-celled urethane foams, used in motorsport, automotive and aerospace fields. The set-up of the indentation test for the absorber made of pure foam is shown in Figure 1-A. The foam mass in the absorber was 43.1 g. The specimen was constrained between aluminium guides to prevent lateral buckling of the foam block during the indentation. The deformed specimen at the end of the quasi-static test is shown in Figure 1-B.

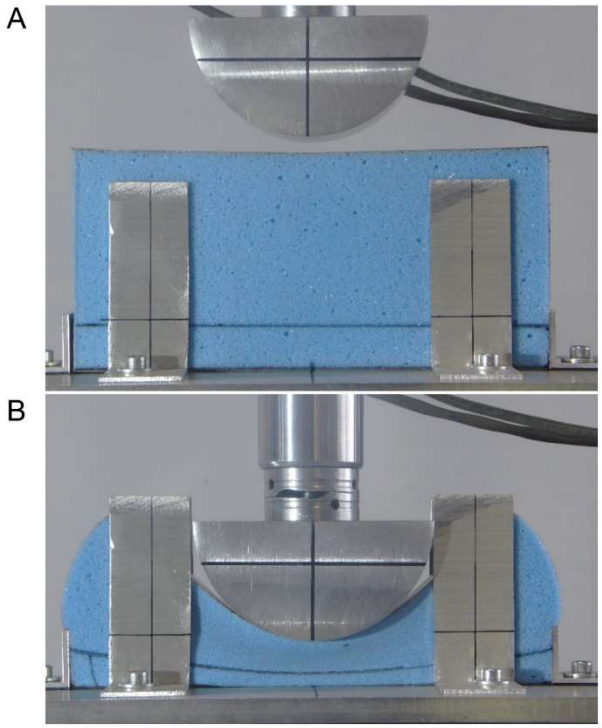

Figure 1 – Indentation tests on foam absorber: (A) lay-out, (B) deformed configuration in quasi-static test

The design of the chiral frame is presented in Fig. 2-A, showing the main dimensions. Chiral topologies consist of a non-centrosymmetric tessellation made of nodes connected by ligaments [38]. The geometry selected was based on thick-walled hexagonal nodes, almost solid with an inner hexagonal hole to reduce the overall weight. Such geometry mitigates the risk of failure at the ligament ends, both in tension and in compression, as discussed in [35]. Moreover, the stiffness of the nodes is also increased, so to enhance the auxetic behaviour, in agreement with the analytical models that prove the auxetic behaviour of chiral lattices [39]. Indeed, the numerical studies carried out in [35] indicate that the adopted geometry is adequate to design hexa-chiral topologies with a Poisson's ratio very close to -1 in elastic range. A further advantage is due to the fact that the triangular spaces external to the hexagons can be filled completely by triangular pre-cut foam inserts without cusps at the corners, thus simplifying the production of foam-filled frames.

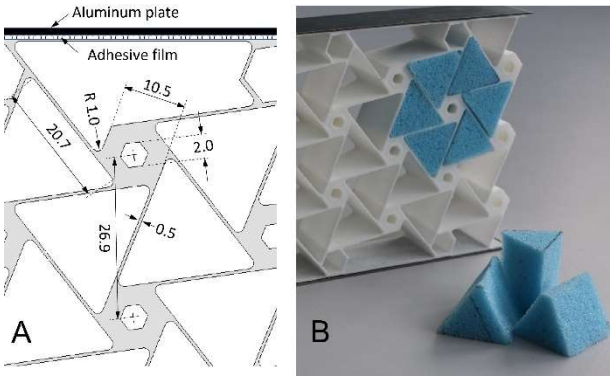

Figure 2– (A) Design of hexa-chiral frame and (B) manufacturing of the foam-filled absorber

The polymeric chiral frames used in the test campaign were laser sintered by using PA 2200 powder produced by EOS Gmbh, based on a polyamide 12 polymer. An example is shown in Fig. 2-B. After some preliminary numerical evaluations, the thick-walled geometry was not

chosen for the nodes in the upper and lower rows. Such nodes were designed with a wall thickness identical to that of the ligaments, to avoid excessive constraints on the deformation of the thin aluminium alloy sheet that reinforced the impacting surface. The difference between the thick-walled and the thin-walled hexagonal nodes can be observed in Fig. 2. The total mass of the polymeric frame was 81 g. Such value does not take into account the mass of the aluminium plate and of the adhesive layer used to bond such plate to the upper surface of the frame, shown in Fig. 2-A, which amounts to 10 g. The average density of the homogenized cellular structure represented by the chiral frame resulted 181.6 kg/m^3. The chiral specimens were tested with the same lay-out used for foam elements, including the presence of the vertical aluminium guides to guarantee the same boundary conditions.

Manufacturing of the foam-filled frame was carried out by cutting prisms of foam with a professional foam cutter and inserting them manually into the triangular spaces between the ligaments, as presented in Fig. 2-B. No adhesive was used between the inserts and the chiral frame. The total mass, excluding the Al plate and the adhesive set between the plate and the upper surface of the frame, resulted in 125 g. The mass of the foam inserts was about 26 g, which is lower with respect to the foam element mass, due to the space occupied by the nodes and ligaments. An average density of 239.5 kg/m^3 was evaluated for this case. The chiral frame and the completed foam-filled absorber are presented in Fig. 3, during the tests, which were performed with the same lay-out as for the foam element, including the vertical aluminium guides.

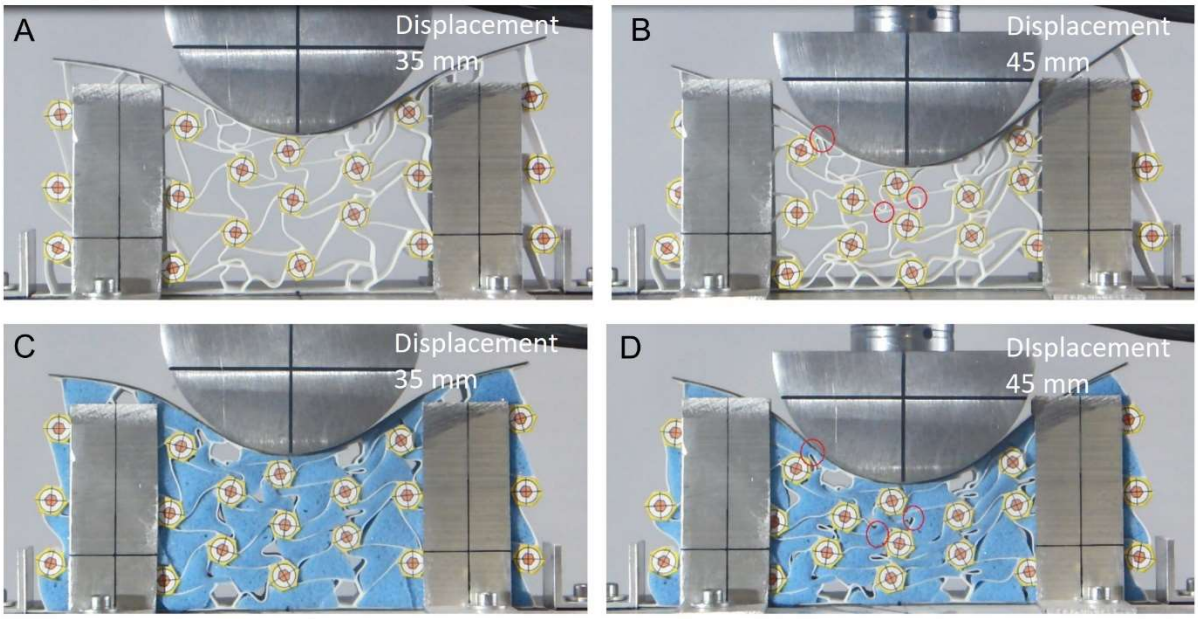

Figure 3 – Deformation in quasi-static indentation: (A,B,) chiral frame, (C,D) foam-filled absorbed

2.2 Results and discussion

The collapse mode of the chiral frame and of the foam-filled absorber in the quasi-static test is presented in Fig. 3 at two increasing displacements of the indenter, namely 35 mm and 45 mm. The auxetic effect given by the chiral frame avoids the transversal expansion of the absorbing material, which was evident in the foam element under the same test conditions, as presented in Fig. 1-B. In the initial phase of the indentation, the collapse modes of the frame and of the foam-filled absorber are almost identical and are characterized by the onset of ligament buckling (Fig. 3-A,C). Some differences can be observed as the indenter entered into the absorbers, because the densifying foam supported the ligaments in the final phase of buckling and prevented their mutual contact. Three examples are evidenced by the red circles in Fig. 3-B,D, but similar phenomena can be observed in several other areas. The deformed configuration presented in Fig. 3-B,D, shows also that the three central nodes of the frame

remained aligned during the indentation. The mutual contact of such hexagons led to a premature peak in the force vs. displacement curves obtained in the tests, shown in Fig. 4.

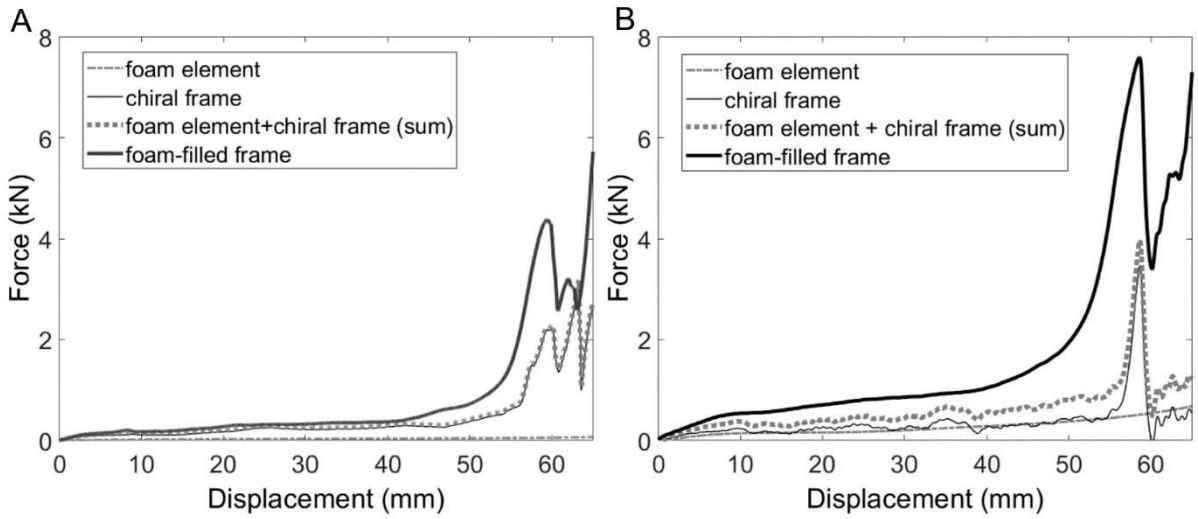

Figure 4 – Comparison of force vs. displacement curves in indentation tests: (A) quasi-static, (B) dynamic

The force vs. displacement curves obtained in the quasi-static tests performed at 1 mm/s are shown in Fig. 4-A. It is apparent that the chiral frame collapsed at an almost constant load level until a load peak at about 55 mm of indenter displacement, which was caused by the mutual contact of the three central hexagonal nodes. In the elements made of pure foam, densification occurred at higher displacements than the maximum ones visualized in the plots, as it will be shown in the characterization of foam material presented in section 3. The sum of the force responses from the foam element and the chiral frame is also plotted in Fig. 4-A. This sum can be compared with the force obtained in the test of the foam-filled frame, which is significantly higher. Such comparison is aimed to provide a first quantitative evaluation of the performance increment that can be obtained by the foam-filled configuration, due to the interaction between the foam material and frame structure. Indeed, the amplification effect on the indentation strength can be attributed to the local densification of the foam triangular prisms confined by the auxetic frame and to the supporting effect of the foam on the buckling of chiral ligaments.

In the response of the tests performed at an indenter speed of 500 mm/s, presented in Fig. 4-B, the plateau force during the indentation of the chiral frame remained almost identical to that of the quasi-static case, though the load peak at 55 mm is more evident and the curve is more irregular. Indeed, dynamic failure mode is characterized by brittle failure of ligaments during buckling, as it can be observed in Fig. 5-A. As a consequence, most of the ligaments in the central zone of the frame were broken during the test, as evidenced in the picture of the indented specimen after the test shown in Fig. 5-B. On the contrary, the force levels in the dynamic indentation of the foam element increased for one order of magnitude with respect to the quasi-static test, thus exhibiting a remarkable strain rate sensitivity. The supporting effect of the foam on the ligament and the auxetic densification of the material under the indenter led to a much higher force response of the foam-filled frame in dynamic conditions, which is noticeably higher than the sum of the forces related to the separate constituents in all the phases of the dynamic tests.

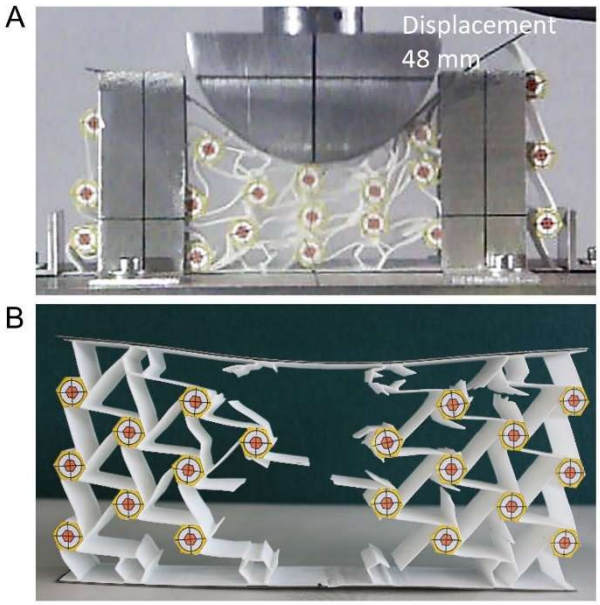

Figure 5 – Dynamic test on the chiral frame: (A) snapshot during indentation, (B) specimen after test

The energy absorption capabilities of all three types of absorbing elements are summarized in Table 1. The energy absorption was evaluated at 50 mm of displacement, before the occurrence of contact events among the central nodes of the frame. The increment of energy, Δ_{energy}, was calculated considering the performance of the foam-filled frame with respect to the sum of energies absorbed by the elements made of a single material. A more rigorous comparison is presented, by defining a a Specific Absorbed Energy (SEA), which was evaluated on the basis of the absorber mass displaced by the indenter, considering the average density of the different absorbers. The increment of SEA, Δ_{SEA}, refers to the performance of the foam-filled frame with respect to simple chiral frame.

All the quantitative indices confirm that the combination of the foam and the auxetic frame significantly improves the performances achieved by absorbers made by single materials. Improvement could be maximized by finding an optimal combination and geometries, which have to be identified for each application scenario, considering specific requirements related to impact energy, indenter shape, available displacement and maximum force levels.

Table 1 – Energy absorption performance of absorbers tested for an indentation of 50 mm

v	Foam		Chiral Frame		Foam-filled frame		Δ_{energy}	Δ_{SEA}
(mm/s)	E (J)	SEA (J/kg)	E (J)	SEA (J/kg)	E (J)	SEA (J/kg)	(%)	(%)
1	1.39	147.5	9.54	535.1	15.23	647.8	39.30	21.07
500	9.73	1032.4	11.95	670.3	40.51	1723.2	87.00	157.09

3. Development of a numerical approach

3.1 Calibration and validation of foam material model

Numerical models of dynamic tests performed on the absorbers were developed using the Simulia/Abaqus Explicit solver in order to prepare an approach for the analysis and prediction of foam-filled auxetic frames. The characterization of foam response was a fundamental part in the development of the models. Indeed, the development of a reliable model for the Conform® foam required the accomplishment of additional compressive tests, performed on foam parallelepipeds with a cross section of 100 mm x 52 mm and an height of 50 mm. Specimens were uniformly crushed between two rigid plates by using an MTS 858 Minibionix II system at a crosshead speed of 2 mm/min, 250 mm/s and 500 mm/s. The data obtained from such tests were used to define three stress vs. strain curves at different strain rates, shown in Fig. 6, which were used in the form of tables to calibrate a material model available in the solver code, specialized for low density foams with strain rate sensitivity *(*Low Density Foam* material [40]). The material model interpolates such tables and provides the stress response as a function of the strain and of the strain rate. The last point in the curve defined for the strain rate of 10 s^{-1} was actually extrapolated from available data to provide a better control of the densification phase at high strain rate.

Moreover, another dynamic indentation test was taken into consideration, which was performed on a 230 mm x 110 mm x 25 mm foam specimen at an impact speed of 250 mm/s, by adopting a different indenter, but the same lay-out as shown in Figure 1, including the vertical guides and the lateral supports. In this test the 100 mm diameter indenter was substituted with a smaller 15 mm diameter cylinder mounted on a fork fixed to the moveable crosshead of the test system. A 0.5 mm aluminium plate was bonded to the upper and lower surface of the foam element, as in the tests performed with the bigger indenter.

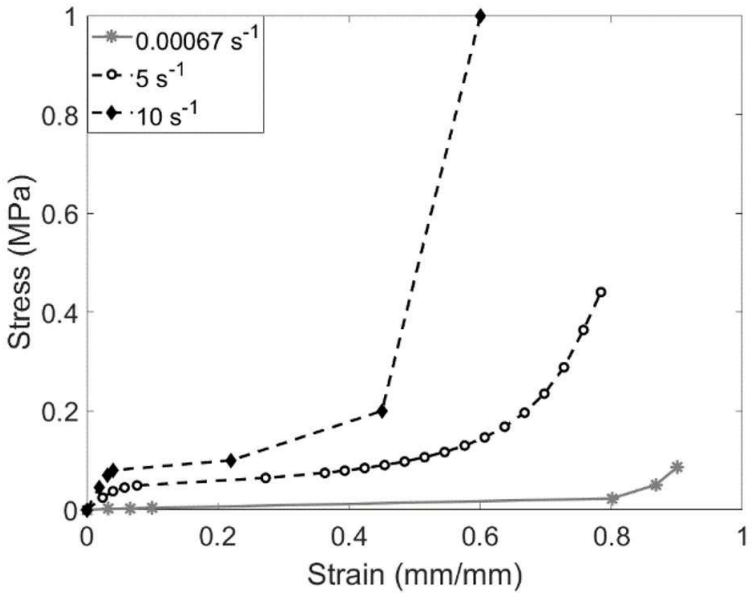

Figure 6 – Stress vs. strains curves at increasing strain rates adopted to characterize the foam material model in numerical analyses

The three models of a uniformly crushed specimen and of two dynamic indentation tests performed on pure foam specimens were developed and solved with Simulia Abaqus/Explicit, considering the physical density of the foam and the actual impact speed of the impactors. The specimen uniformly compressed in the crushing test was modelled by 4225 hexahedral elements with reduced integration scheme (*C3D8R* elements [40]), with a typical size of 4 mm. The top and bottom surfaces of the deformable mesh were set into contact with a moveable and with a fixed rigid surface, respectively, made of rigid shell elements (*R3D4* elements [40]). The contour of displacement magnitude shown in Fig. 7-A is referred to the crush analysis performed at 250 mm/s. A two-dimensional model of the dynamic indentation with the 15 mm diameter indenter was also developed, as shown in the contour of displacement magnitude presented in Fig. 7-B. Only a one-element wide slice was represented by using 4863 elements (*C3D8R* elements [40]) in order to validate the material model for the same type of finite element that will be used in further research. The depth of slice was 0.5 mm, whereas the typical

dimension of the elements in the plane of the slice was 2.5 mm. Symmetry constraints were used on one side of the model to avoid any displacement out of the plane of the modelled slice. On the other side, the contact with the vertical aluminium guides was established. The edges were also set in contact with the models of the lateral supports, to accurately represent the test lay-out shown in Fig. 1.

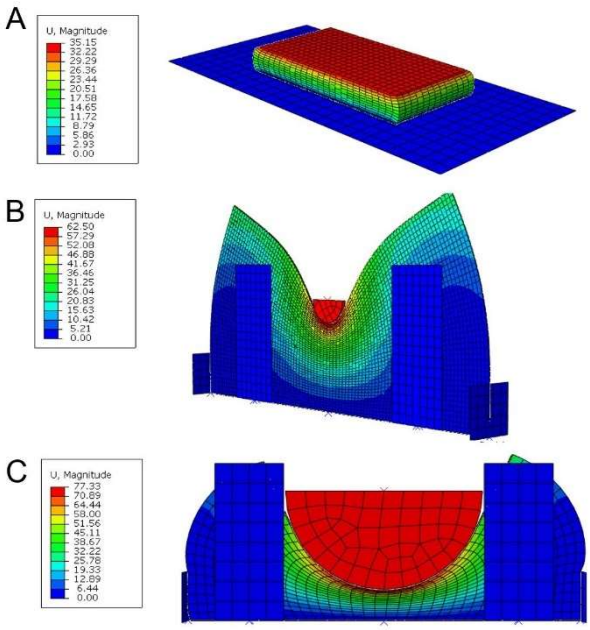

Figure 7 – Numerical analysis of (A) crush test at 250 mm/s, (B) dynamic indentation at 250 mm/s with 15 mm diameter indenter, and (C) dynamic indentation with 100 mm diameter indenter at 500 mm/s

All the aluminium parts were modelled by using an elastic-plastic material model with a Young modulus of 70 GPa, a Poisson's ratio of 0.3 and a yield stress of 300 MPa. Finally, the model of the test performed with the 100 mm indenter is presented in Fig. 7-C, where contours of the displacement magnitude are shown. A one-element wide slice, with a width of 1.0 mm, was modelled by using hexahedral C3D8R elements with a typical size of 5 mm in the plane of the slice. Boundary conditions and material models were identical to the ones used in the model of

the test performed with the small indenter. It can be observed that the deformed shape shown in Fig. 7-C is in good agreement with the experimental evidence reported in Fig. 1.

The numerical-experimental correlation of the force vs. displacement curves obtained in the three abovementioned analyses is shown in Fig. 8. It can be seen the foam model provided appreciable results in all considered conditions. Densifications occurred at different displacement levels for the three tests and this aspect is accurately represented by the models. In the analysis of the dynamic test performed with a 100 mm diameter indenter, the energy absorbed at an indentation of 50 mm was of 9.68 J, with a discrepancy of 0.52% with respect to the experimental value. Overall, the foam material model can be adopted for a reliable estimation of the response in the foam-filled absorbers.

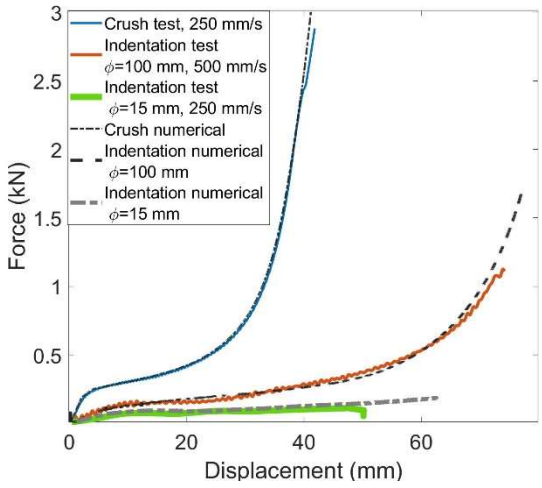

Figure 8 – Numerical-experimental correlation in the tests performed on pure foam elements

3.2 Numerical model of absorbers with auxetic frames

The FE model of the polymeric chiral frame was developed considering a slice with a width of 1.0 mm, as shown in Fig. 9-A. The ligaments and the external borders of the hexagonal frame were modelled by shell elements with a reduced integration scheme (*S4R* [40]) and a typical size of 1 mm. The upper and lower plates were separately modelled and connected by using a

TIE algorithm, available in the solver code to join dissimilar meshes. A general mutual contact interaction was introduced among all elements, with a friction coefficient of 0.2, in agreement with the values used for the analyses of tubes filled by polyurethane foam in [41]. The internal parts of the filled nodes were meshed by solid hexahedral elements (*C3D8R* [40]). The indenter and the lower ground surface were modelled by rigid elements included in the general contact interaction. A total number of 4344 elements were used.

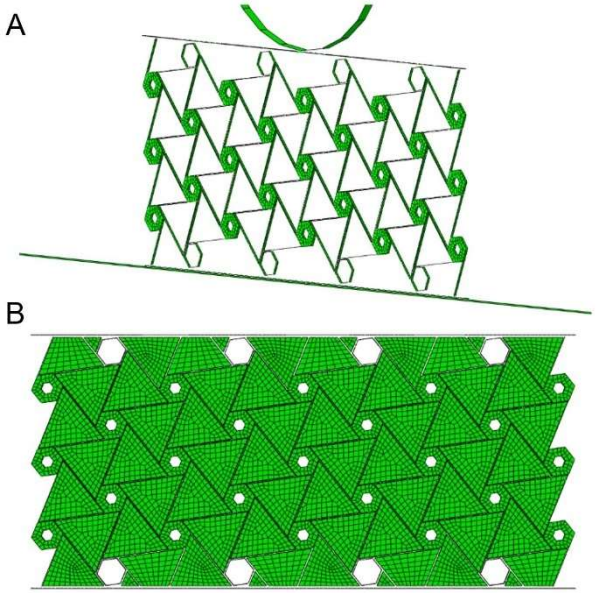

Figure 9 – Numerical models of (A) chiral frame, (B) foam-filled absorber

A fixed vertical velocity of 500 mm/s was prescribed to the reference node of the rigid body representing the indenter. A symmetry constraint was imposed to all the nodes at one side of slice, in order to prevent lateral displacement, whereas preliminary analysis indicated that there was no need for modelling the vertical guides used in the test lay-out.

The PA2200 polymeric material was represented by an elastic-perfectly plastic material model, with a yield stress of 48 MPa, set according to the material datasheet provided by material supplier. A damage was activated at a plastic strain of 10% to model material failures (*ductile damage initiation criterion* [40]). Strain rate dependency was modelled by applying a trial and

error procedure, which led to acceptable results by increasing the yield strength and by reducing the plastic strain at damage initiation by a factor of 2 at a strain rate of 2 s^{-1}. The upper surface of the frame was modelled as a laminated material constituted by a layer of PA2200, a layer of epoxy adhesive, with E=1500 MPa and $v=0.3$, and a 0.5 mm thick layer of aluminium alloy sheet, characterized as in the model of pure foam absorbers.

The numerical model of the foam-filled frame was developed by introducing the meshes of the triangular foam prism in the model of the chiral frame slice, made of hexahedral elements (*C3D8R* [40]), as show in Fig. 9-B. The foam was characterized by using the material model calibrated in the previous sub-section and the foam elements were included in the general contact among all the external surfaces of the parts constituting the model.

3.3 Numerical-experimental correlation for absorbers with auxetic frames

The collapse mode of the chiral frame and of the foam-filled absorber are shown in Fig. 10, where the contour of displacement in the horizontal direction x is reported to evaluate the contraction of the material obtained due to the auxetic behaviour of the frame. The deformed shape of the chiral frame, presented in Fig. 10-A is in good agreement with the experimental evidence reported in Fig. 3. Damage developed in the elements at the cusps of the sharply buckled ligaments, so that ligament breakage is predicted with an acceptable accuracy. Displacements in x direction have positive values at the left side and are negative at the right side, thus indicating an evident contraction of the frame. The collapse mode of the foam-filled absorber is also in an acceptable agreement with the experimental results, as it can be observed by comparing the Fig. 10-B with the Fig. 3. Foam prisms in the model were highly compressed by the collapsing ligaments, with the development of gaps where the foam was not able to flow in the space created by ligament buckling. The auxetic behaviour is less evident than in the case of the unfilled chiral frame, since the foam expansion opposed to the contraction of the frame.

Such phenomenon indicates, at the macroscopic level, the presence of an effect of the foam on the deformation, and the subsequent collapse, of the frame ligaments.

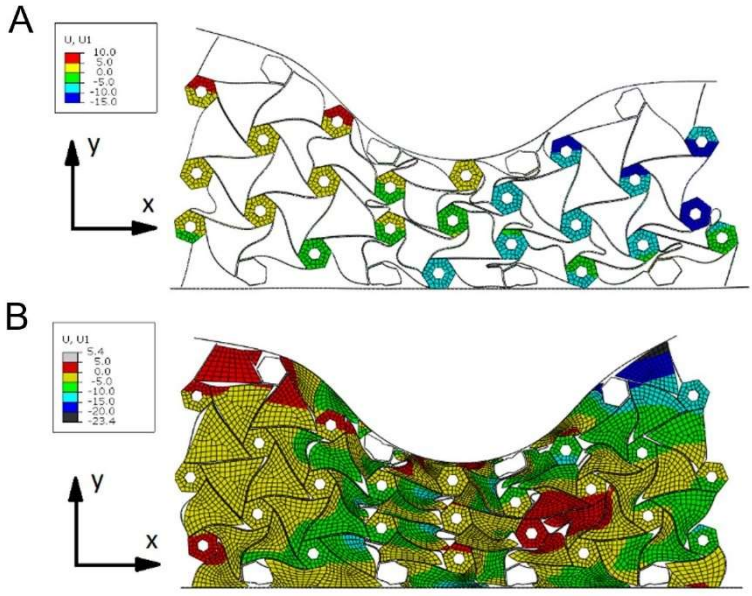

Figure 10 – Numerical contour of horizontal displacement at 50 mm of indenter displacement: (A) chiral frame, (B) foam-filled absorber

The quantitative numerical-experimental correlation is presented in Fig. 11. Both numerical models did not capture the occurrence of the force peaks due to contact of the three centrally aligned polygonal nodes, which occurred at 55 mm and 50 mm for the chiral frame and the foam-filled absorber, respectively. Such phenomenon, which was described in the discussion of the text results in section 2.2, is not completely modelled in the numerical analyses. Indeed, in the analysis of the chiral frame, the three nodes lost the alignment in the initial phases of the collapse, whereas, in the analysis of the foam-filled absorber, contact occurred without producing a peak, since the nodes slid apart during the interaction. Despite such discrepancy, the correlation up to 50 mm of indenter displacement is appreciable. The initial ramp followed by a plateau in the chiral frame and by a linearly increasing force level in the foam-filled frame are captured with a good accuracy. Overall, the results indicate that the modelling approach

provided realistic predictions of the response of the chiral frames and the foam-filled chiral frames in dynamic indentation and localized impacts.

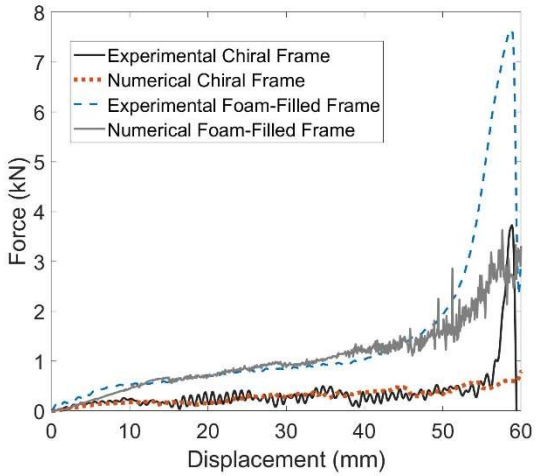

Figure 11 – Numerical-experimental correlation of force vs. displacement response for absorbers with auxetic frames

4. Numerical studies of absorbers with optimized frame response in plastic range

4.1 Definition of a general objective for optimization of frame behaviour

The auxetic response of the chiral frame played a fundamental role in the performance of the foam-filled element presented in the previous section. The frame deformation opposed to the lateral expansion of the foam, despite the progressively increasing volume occupied by the penetration of the indenter. A direct consequence is that more material was involved in deformation process. Moreover, the auxetic effects helps the local densification of the foam, which interacted and supported the frame ligament during collapse, thus resulting in failure modes more efficient for energy absorption.

It must be observed that, in the application considered, the chiral frame worked mostly in plastic range. Moreover, experimental tests and numerical results showed that ligaments were subject to the development of plastic hinge and to failures beyond certain strain levels, so that the frame locally lost the ability of contraction under indentation. According to such observations, the optimization of the auxetic response in the elastic range is not adequate to provide the best geometries for the energy absorption performance of a foam-filled chiral frame. A more appropriate objective could be the increment of the maximum contraction achievable in plastic range, before the occurrence of any failure in the ligaments. Such objective is actually quite general and independent of the combination of materials selected for the absorbers and of the specific requirements of the application scenario. Indeed, the geometries identified through such approach, could be adopted to enhance the performance of a generic foam-filled frame. Moreover, such geometries could be scaled, so to fulfil different requirements related to specific impact scenarios, such as the maximum allowable force levels, the impact energy, and the available crushing depth. Finally, a study regarding auxetic behaviour of chiral structures undergoing plastic deformation has never been conducted so far in literature and is retained of particular interest to achieve a better insight on the design rules of energy absorbers based on auxetic frames.

Some aspects regarding material selection and the details of chiral geometries were also reviewed, considering the experimental results:

- the 3D printed polymeric material exhibited a remarkable strain rate sensitivity and a brittle behaviour at high strain rate; such behaviour is not desirable and would have a strong influence on the result of the optimization process, so that a different material could be more adequate to perform the optimization process;

- the use of thick-walled nodes increased the mass and led to premature load peaks due to mutual contact between nodes; a pre-determined thickness is no more needed if an optimization process identifies the optimal thickness of the nodes to maximize the contraction before failure;

Accordingly, the optimization process took into account hexachiral frames with circular hollow nodes made of Additive Manufactured Titanium alloy, which exhibit a much lower strain rate sensitivity and adequate ductility. Indeed, despite the porosity and orthotropy effects of AM process, titanium alloy sheets produced by Addictive Manufacturing technique, such as SLS or EBM, may exhibit strain at failure in plastic range up to 7%÷8% [42].

The optimization was based on the non-linear static analysis of the compressive response of a 7-nodes chiral unit, which was selected to be easily analysed and for the suitability to future experimental testing. The unit, with a height H and a width W, is shown in Fig. 12. During the analysis, the lateral contraction of the unit was measured by the displacement δ_h, which was obtained as the difference of the displacements at the virtual centres of the two lateral nodes. The plastic strains developed on all the ligaments were monitored, so that when the maximum plastic strain in the unit, ε^p_{max}, exceeded a pre-defined allowable, ε^p_{lim}, the corresponding contraction was stored as $\delta_{Aux\text{-}Fail}$. This made possible the implementation of an optimization process aimed to maximize the ratio $\delta_{Aux\text{-}Fail}/H$, which was considered a significant measure of the auxetic effect in plastic range for a given geometry, before the occurrence of any ligament failure.

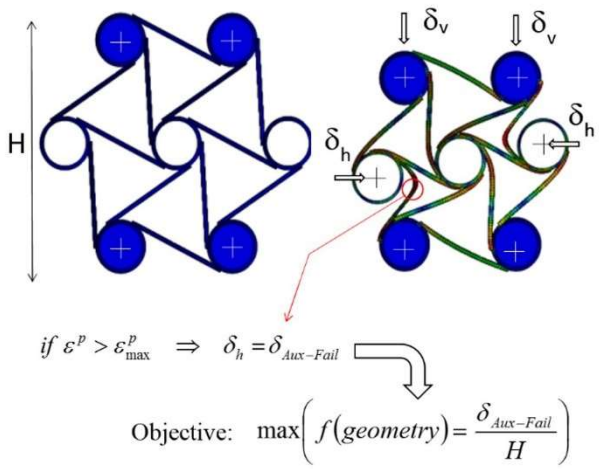

Figure 12 – Chiral unit considered for optimization and objective function

4.2 Parameterized models

The optimization process was conducted for three values of the height *H* of the chiral unit shown in Figure 12, namely *H* = 34 mm, *H* = 68 mm and *H* = 136 mm. The width of the units, *W*, was set to 5 mm, 10 mm, and 20 mm for the three values of *H*, respectively. A Matlab® script was developed to generate the mesh of the units, by using bi-linear shell elements (Type *S4* - [40]). Models were characterized by the set of geometrical parameters shown in Fig. 13-A, which also included the thickness values of the ligaments and of the nodes. Tapered ligaments were considered with the aim to achieve a more uniform distribution of strains during ligament deformation and delay failure. From the technological point of view, such tapering could be easily produced in additive manufacturing processes.

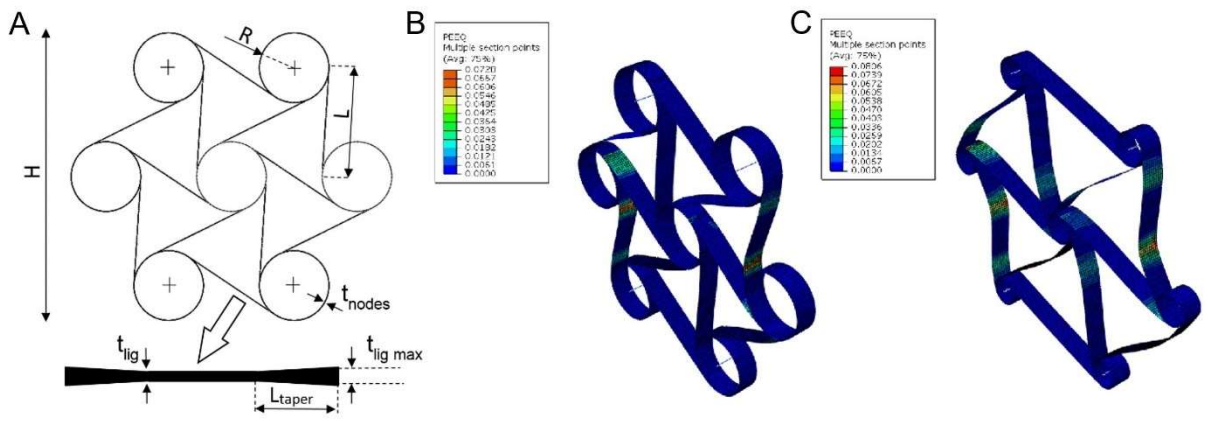

Figure 13 – (A) Design variables in the chiral unit, (B) numerical analysis of a chiral unit with low L/R, and (C) numerical analysis of a chiral unit with high L/R

The design variables in the optimization processes were defined by using or combining the geometrical parameters shown in Fig. 13-A and are summarized in Table 2. The ranges indicated were adopted for all three optimization processes with different heights *H*. An absolute limit was set to 0.50 mm for the minimum thickness to obtain technologically feasible solutions, since such parameter is typically limited in additive manufacturing processes.

Table 2 – Design variables in the optimization of the chiral unit

Design Variable	Expression	Range
Ligament length to node radius ratio	L/R	3 ÷ 10
Nodal thickness	t_{nodes}	0.5 mm ÷ 3.0 mm
Ligament thickness	t_{lig}	0.5 mm ÷ 2.0 mm
Percentage of tapered zone	$T_{\%} = \left(L_{taper} - L\right)/L \cdot 100$	0.0% ÷ 40.0%
Taper ratio	$\Delta t = t_{lig\,\max} - t_{lig}$	0.0 mm ÷ 1.0 mm

The models presented in Figure 13-B and Figure 13-C are based on two different meshes produced automatically by the Matlab® procedure.

The motion of the upper and lower nodes of the samples was coupled to the displacement of four pins, modelled by beam elements, which are visible in Fig. 13-B. A kinematic coupling was introduced among the nodal degrees of freedoms of the pins and those of the finite elements belonging to the chiral nodes, which were allowed to rotate freely about the pin axes but were forced to follow the axis translation. A downward displacement was imposed to the axes of the upper pins, while the lower ones were kept fixed in the vertical direction. Horizontal displacements were kept fixed for all the pin axes. All shell elements were described by a thickness according to the parameters given in Table 2. An isotropic elastic-plastic material model was used, with a Young Modulus of 105 GPa and a Poisson's ratio of 0.3. The yield stress was set 768.1 MPa and the ultimate engineering stress was set at 854.6 MPa, at a total strain of 7.60%. Such values are representative of a Titanium Al6V4 alloy, produced by 3D printing [43]. A true stress – true strain curve was defined under the assumption of a Poisson's ratio of 0.5 in plastic range to properly characterize the material for non-linear analyses.

Non-linear analyses were performed by Simulia/Abaqus Standard code, by imposing a final downward vertical displacement equal to 20% of the initial height. Results were post-processed to monitor the plastic strain in the ligaments and to identify the horizontal contraction $\delta_{Aux\text{-}Fail}$. A convergence study was performed to check the reliability of the stress field, and meshes with more than 50 elements along each ligament were considered adequate. After preliminary analyses, a contact interaction was set among the surfaces of the ligaments and the nodes, to avoid interpenetrations in compression.

The models presented in Figure 13-B and Figure 13-C are representative of units with low and high L/R ratios, respectively. The contour of plastic strain in Fig. 13-B indicates that, with low L/R, plastic hinges tend to develop at the end of the ligaments, close to the nodes, whereas units with high L/R tend to fail by developing plastic hinges in the middle of the ligaments, as presented in Fig. 13-C.

Preliminary analyses revealed the validity of a scaling law for the responses of the chiral units in the linear and non-linear range. The curves reported in Fig. 14-A are referred to chiral units with L/R = 5.0, fixed ratios between ligaments length and ligaments and nodal thickness (L/t_{lig} = 30, L/t_{nodes} = 20), and no tapering, but with different heights. Responses were characterized by a yielding, followed by a peak and a subsequent softening regime, until a contact between the buckled ligaments and the nodes was achieved, towards the end of the analyses. If the forces are normalized with respect to a reference area given by $H \cdot W$ and the displacements are normalized with respect to H, the curves can be perfectly superimposed, as shown in Fig. 14-B. Moreover, the normalized performance index, $\delta_{Aux\text{-}Fail}/H$, were identical for all the three curves. Thanks to the scaling law, performing the optimization processes for different height could have been considered redundant, but the technological absolute limit set on the minimum thickness achievable by additive manufacturing process actually led to different optimal solutions for units having different dimensions.

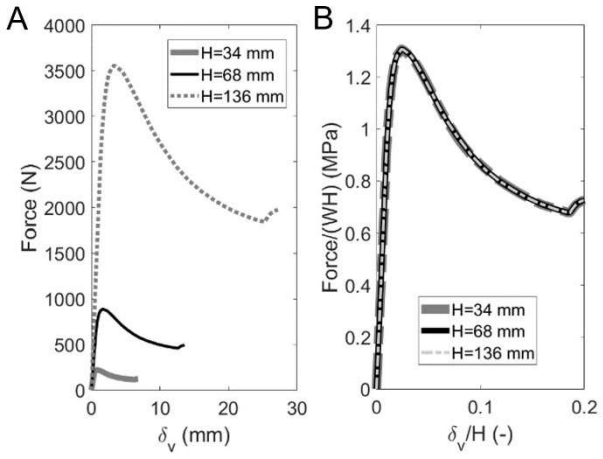

Figure 14 – (A) Force-displacement numerical response of chiral unit with different heights and (B) normalized responses

3.3 Implementation of the process and results

The *Optimax* software package developed at University of Maribor [44] was used to implement the optimization process. A genetic algorithm was adopted, with control parameters that were adjusted by means of preliminary trials performed on a unit with H=68 mm, which converged towards a solution that maximized $\delta_{Aux\text{-}Fail}$ after 12 generations. The control parameters adopted to obtain the results presented in this sub-section are indicated in Table 3.

Table 3 – Control parameters of genetic algorithm

Parameter	Value
Population	50
Number of generation	30
Crossover rate	0.8
Mutation rate	0.05
Elitism	Implemented

The samples generated during the optimization process were used to create response surfaces, by using the Delaunay triangulation and natural neighbour interpolation method provided in Matlab® code.

The section of the response surface for the unit with H=34 mm and reported in Fig.15-A shows that the $\delta_{Aux\ Fail}/H$ index is maximized in a region with L/R = 3÷4 and a tapered zone extended for 10% of the ligament. The influence of ligament thickness is significant, as shown in the results reported in Fig. 15-B, and optimal solution was actually found on the frontier of the variability range for the L/t_{lig} ratio, at L/t_{lig}. ≈ 25. Hence, the limit to the minimum value of t_{lig}, set to 0.5 for technological reasons, played an important role in the optimization process. This is confirmed by the results obtained for the unit with H = 68 mm, which are shown in Fig. 16. Indeed, the optimal values of L/R are close to the previous ones and the optimal solution is again at the frontier of L/t_{lig} ratio range. For this case, the optimal L/t_{lig} is about 50 and the maximum value of objective function is higher than that of the cell with H = 34 mm. In the optimization process with H = 136 mm, the optimal solution was found inside the design space, as shown in Fig. 17. The optimal tapering parameter remained unchanged to about 10%, while the L/R ratio was close to 5. An optimal L/t_{lig} ratio of 110 was found, corresponding to a t_{lig} = 0.54 mm.

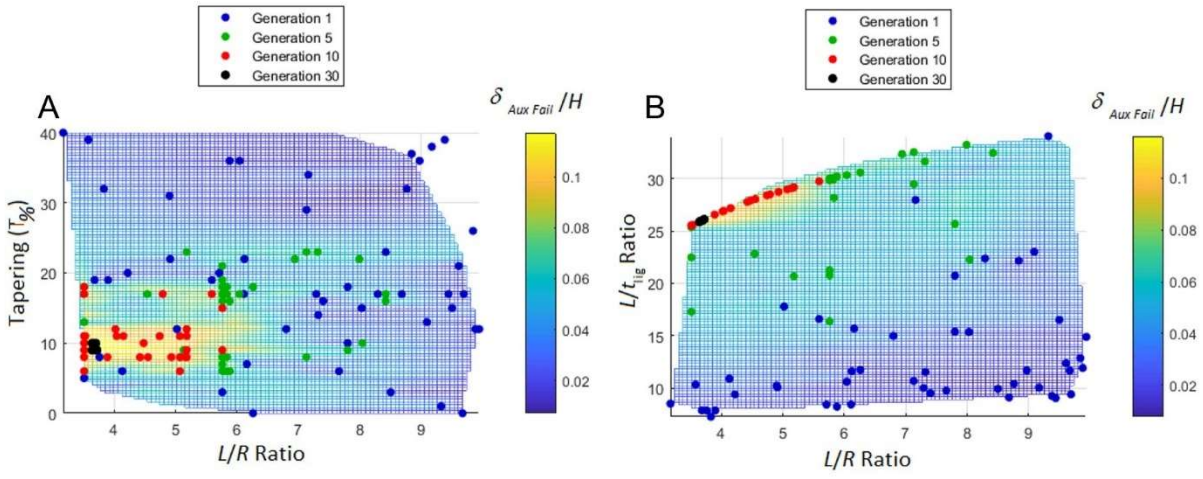

Figure 15 – Sections of response surfaces for the chiral unit with H=34 mm: (A) in the T%-L/R plane, (B) in the L/t_{lig}-L/R plane

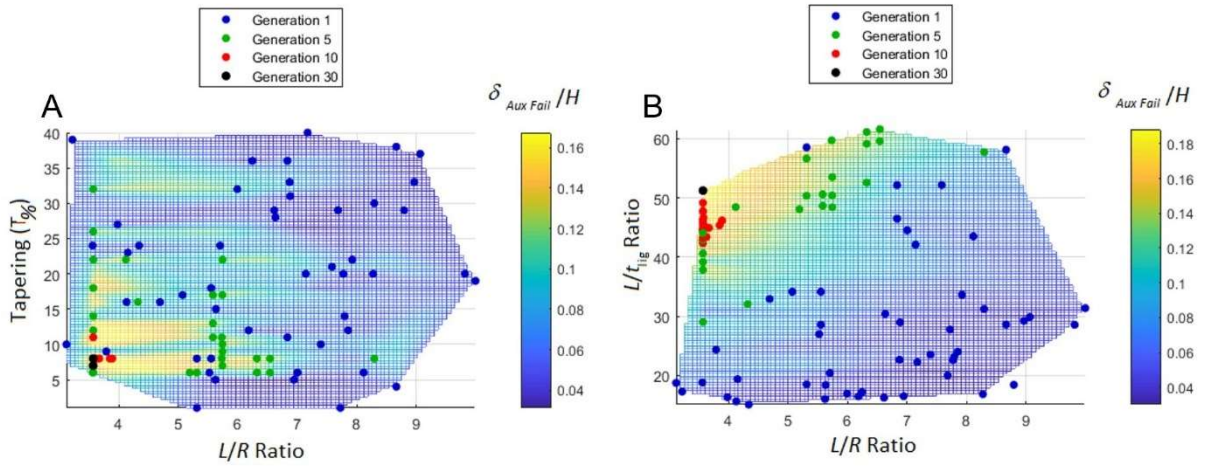

Figure 16 - Sections of response surfaces for the chiral unit with H=68 mm: (A) in the T%-L/R plane, (B) in the L/t_{lig}-L/R plane

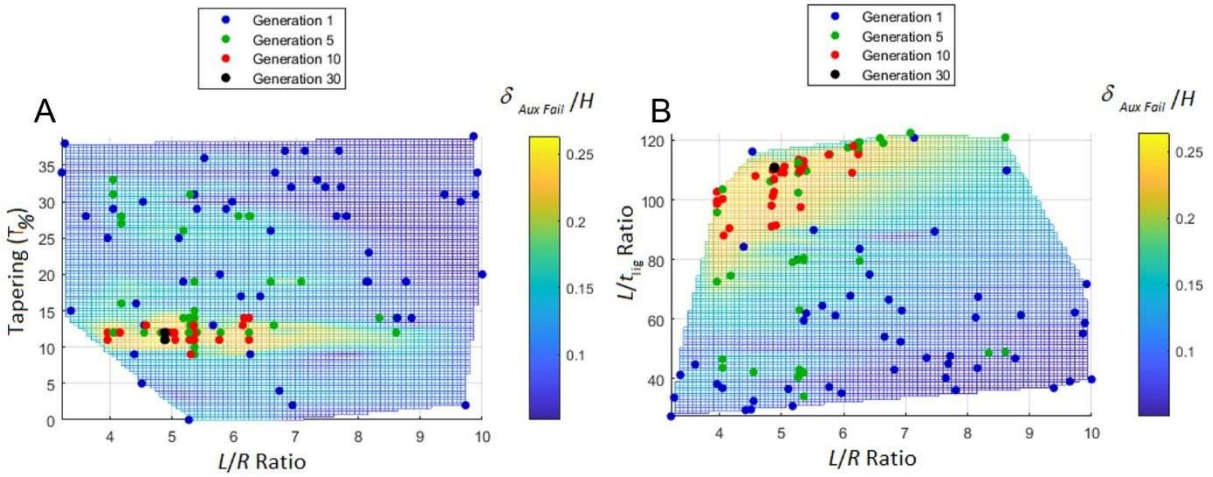

Figure 17 - Sections of response surfaces for the chiral unit with H=68 mm: (A) in the T%-L/R plane, (B) in the L/t_{lig}-L/R plane

The average values of parameters identified in the last generation of the genetic algorithm are reported in Table 4. Overall, it can be observed that a high L/t_{lig} ratio is required to delay the ligament failure, so to maximize the contraction capability of the chiral frame. Sensitivity

analyses do not reveal a large influence of the t_{nodes} parameter, after a certain threshold. Therefore, maximum contractions can be achieved with relatively thin nodal thickness, thus allowing a significant weight saving. Thickening of the ligament thickness at the end is desirable for about 10% of the length. However, such indication is likely to be influenced by the local solution of the shell model at the intersection between nodes and ligaments, which cannot be considered totally reliable.

For the specific material selected, optimized units may achieve a contraction in plastic range between 10% and 26% of the initial height, without exceeding the failure limit. The gain with respect to a randomly selected configuration can be as high as 300%.

Table 4 – Optimized parameters and optimal results obtained by the genetic algorithm

H (mm)	L/R	L/t_{lig}	t_{nodes} (mm)	t_{lig} (mm)	$T_{\%}$ (%)	Δt (mm)	$\delta_{Aux\,Fail}/H$
34	3.68	26.0	2.63	0.51	9.5	0.11	0.116
68	3.57	51.3	1.19	0.51	7.5	0.11	0.189
136	4.89	110.8	2.04	0.54	11.5	0.88	0.269

3.4 Numerical simulation of foam-filled metallic chiral frames with enhanced geometries

The optimization performed proved that it is possible to improve the capability of an auxetic frame to contract in plastic range, thus contributing to densification of the material under the indentation. This represents a first step in the design of an optimised absorber based on the combination of an auxetic frame combined with an energy absorbing filler, although configurations should be optimized for each specific impact scenario. Moreover, the optimal

combination of materials for the filler and the frame must be defined, carefully considering properties of available materials and the limits of technological processes.

Despite such limitations, the research presented in this paper enabled a numerical evaluation of the performance obtained by applying titanium alloy frames, based on the geometries identified in the previous optimisation study, filled by the visco-elastic polyurethane foam considered in the experimental tests. Results provided an evaluation of the possible advantages that can be achieved by the filler material, even if its mechanical properties are much lower than those of the frame material.

A numerical model of a one-element wide stripe of a foam-filled frame was built in Abaqus software based on an optimised cell geometry determined in previous chapter. The numerical model and boundary conditions are shown in Fig. 18. Bi-linear quadrangular shell elements with a reduced integration scheme (S4R, [40]) with a typical size of 0.8 mm were used for the frame, while three-linear hexahedral elements with reduced integration scheme (C3D8R, [40]) and a size of about 1 mm were used for the foam discretization. The Z-symmetry boundary conditions were applied to the front face of the absorber, while kinematic coupling [40] constraint was prescribed to the transversal translations of the nodes on the back face of the absorber. Coupling ensured that the absorber's frame and foam inserts expand or contract identically in transversal direction, which guaranteed that the absorber remained planar without enforcing a plane strain conditions. This avoided irregular behaviour of the foam and of the contact interactions. General contact interaction with a friction coefficient of 0.2 was used for all the analysed cases [41].

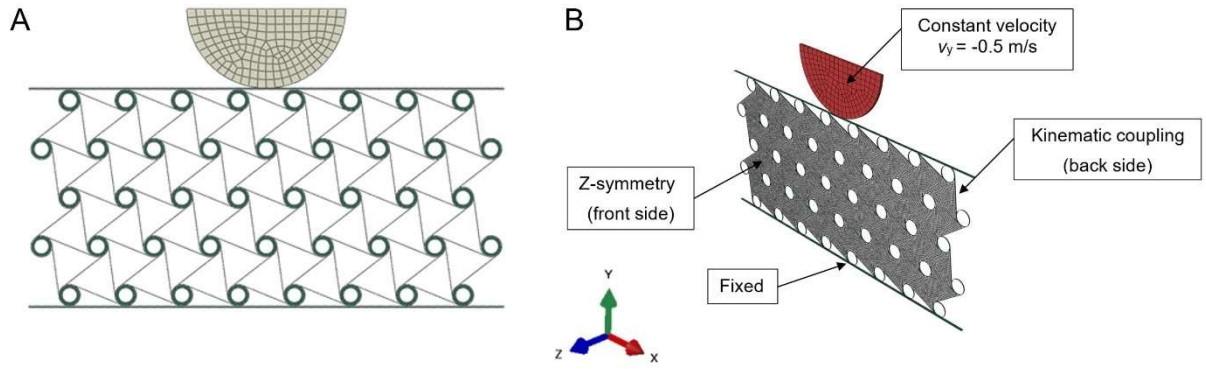

Figure 18 – Geometry of crash absorber (A) and boundary conditions of numerical model (B)

Titanium alloy was used as a material model for the auxetic frame as was used in the optimisation procedure and for the foam inserts the same material parameters as presented in Section 3.1 were used.

The results of numerical simulations are shown in Fig. 19, where the influence of the foam filler can be observed. The initial peak force and general force levels are larger in the case of the foam-filled crush absorber. Response is characterized by a series of force drops, occurring at different displacements for the two absorbers types, which will be further analysed later.

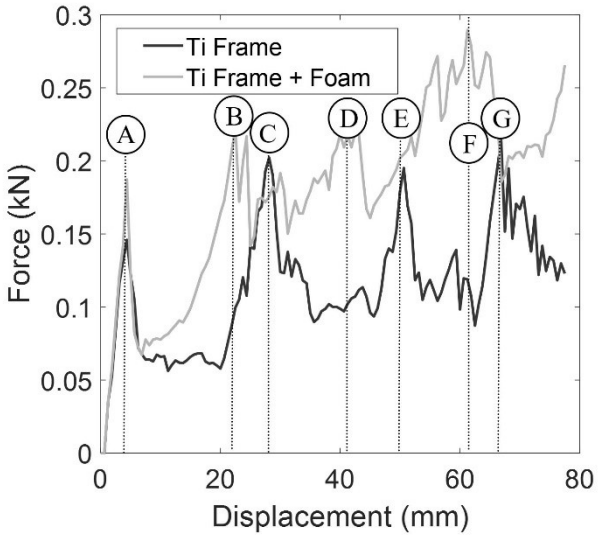

Figure 19 – Comparison of mechanical responses of Ti frame and Ti foam-filled frame

The deformation behaviour of the crash absorber is shown in Fig. 20, where the deformation of Ti frame and foam-filled Ti frame is shown at increasing displacements. The analysis of the crushing mechanism indicates the reason for the recorded force drops after the peaks labelled in Fig. 19. Recorded force drops are a consequence of the ligament buckling that are marked in Fig. 20.

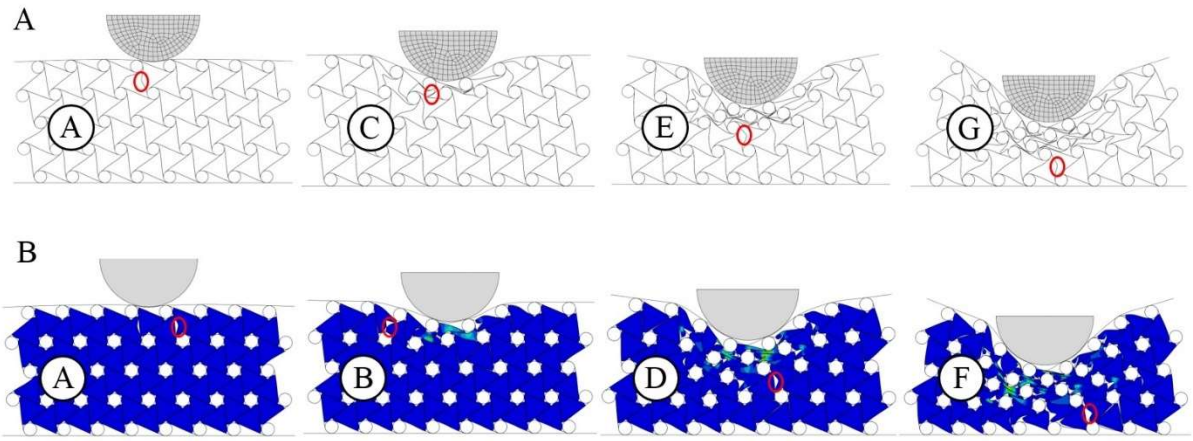

Figure 20 – Analysis of the force drops in Ti frame (A) and Ti foam-filled frame (B)

In this case, the differences between the deformation of the ligaments between the two types of absorbers are not so evident as in the polymeric frame cases, since the foam could provide an adequate supporting force to prevent complete buckling of titanium ligaments. However, the force vs. displacement response in Fig. 19 shows that ligament buckling in the foam-filled frame occurred at generally higher and much more uniform force levels than in the case without the foam.

The results of the energy absorption performance of the titanium crash absorber (extrapolated to a 25 mm wide absorber) were calculated with the same procedure as described in the section 2.2 (Table 1) and are shown in Table 5. The density of the titanium alloy frame equals to

737.9 Kg/m^3, whereas the addition of the foam increased the density to the value of 806.4 kg/m^3.

The energy absorption was evaluated at 50 mm of indentation and the specific energy absorption was based on the volume of material that was displaced by the cylindrical impactor. Results indicate that the foam-filled frame provided an increment of absorbed energy and specific energy of 50 % and 37 %, respectively, compared to the frame alone. The difference in energy absorption performance between the frame and the foam-filled frame is lower than in the case of polymeric frames in dynamic conditions. This can be explained by considering the much lower absolute energy absorbing capability of the foam with respect to the titanium. Accordingly, the densification of the foam cannot provide a significant increment of absorbed energy. However, the presence of the foam led to an increase of energy absorption performance that is higher than that of the polymeric frame in static condition. Such effect is to be attributed to the supporting effect of the foam, which can be particularly significant when the foam is in the densification state.

It should also be observed that the application of the titanium material and of the optimized geometry led to an increase of the SEA values with respect to the original polymeric frame. The increase equals to 212% for the chiral frame alone and to 67% in the case of the frame filled by the identical polymeric foam in the same dynamic conditions.

Table 5 – Energy absorption performance of Ti absorber tested at an indentation of 50 mm

v	Chiral Frame		Foam-filled frame		Δ_{energy}	Δ_{SEA}
(mm/s)	E (J)	SEA (J/kg)	E (J)	SEA (J/kg)	(%)	(%)
500	151.7	2094.1	227.6	2874.8	50.02	37.28

5. Conclusions

Experiments carried out on the polymeric frames showed that auxetic frames based on chiral topologies and energy absorbing foams can be combined to obtain enhanced energy absorption performances in the case of localized impact. The chiral frame helps by densifying the energy absorbing medium close to the contact zones, whereas the foam provides a supporting effect to the ligament of the frame, thus improving its specific energy absorption capability. These findings were confirmed both by indentation tests at different speeds and by the analysis of the numerical models, validated against the experimental results.

The developed numerical approach can be considered as a valid tool to predict the response of the foam-filled auxetic frame under impact and indentation conditions. However, the identification of optimal configuration depends on the specific impact scenario considered and must take into account the possibility offered by available materials and technologies in order to determine the best combination between the frame and the filler materials. A first attempt towards the definition of configurations that could be considered of general validity was carried out by optimizing the capability of an auxetic metallic frame to contract under compression without exhibiting localized failure. The results of the optimization outlined the importance of technological limitations regarding the thickness of the ligament walls, confirmed the validity of scaling laws to evaluate the forces, the compressive displacements and the contractions at failure for differently sized chiral topologies, and indicated the possible advantages coming from the adoption of tapered ligaments. An optimized geometry was adopted to evaluate numerically the energy absorption performance of a Titanium frame filled by a polymeric foam, by adopting the numerical procedure previously validated. Results confirm the enhancement that can be achieved by the supporting effect of the foam even if, in this case, the titanium ligaments buckled at much higher loads than in the case of the polymeric frame.

These results are promising for the further development of the foam-filled auxetic frames and indicates the importance of choosing an optimal combination of frame and foam material. In particular, the research activity points out that innovative energy absorbers, optimized for localized scenarios, could be manufactured by exploiting the possibility offered by the new manufacturing processes. Indeed, additive manufacturing techniques could be used to produce auxetic frames with complex and even graded geometries that could be filled to increase both the force levels required for the frame collapse and the amount of filler material involved in the indentation.

Acknowledgements

The research was partially funded by Slovenian Research Agency (ARRS) in the framework of Research Project No. J2-8186 and the Research Core Funding N0. P2-0063

Data Availability

The raw/processed data required to reproduce these findings cannot be shared at this time as the data also forms part of an ongoing study.

6. Literature

[1] Lehmhus D, Vesenjak M, de Schampheleire S, Fiedler T. From stochastic foam to designed structure: Balancing cost and performance of cellular metals. Materials (Basel) 2017;10:1–32. https://doi.org/10.3390/ma10080922.

[2] Tarlochan F, Ramesh S, Harpreet S. Advanced composite sandwich structure design for energy absorption applications: Blast protection and crashworthiness. Compos Part B Eng 2012;43:2198–208. https://doi.org/10.1016/j.compositesb.2012.02.025.

[3] Yan L, Chouw N, Jayaraman K. Lateral crushing of empty and polyurethane-foam filled natural flax fabric reinforced epoxy composite tubes. Compos Part B Eng 2014;63:15–26. https://doi.org/10.1016/j.compositesb.2014.03.013.

[4] Duarte I, Vesenjak M, Krstulović-Opara L, Ren Z. Crush performance of multifunctional hybrid foams based on an aluminium alloy open-cell foam skeleton. Polym Test

2018;67:246–56. https://doi.org/10.1016/j.polymertesting.2018.03.009.

[5] Duarte I, Krstulović-opara L, Dias-de-oliveira J, Vesenjak M. Axial crush performance of polymer-aluminium alloy hybrid foam filled tubes. Thin Walled Struct 2019;138:124–36. https://doi.org/10.1016/j.tws.2019.01.040.

[6] Duarte I, Krstulović-Opara L, Vesenjak M. Characterisation of aluminium alloy tubes filled with aluminium alloy integral-skin foam under axial compressive loads. Compos Struct 2015;121:154–62. https://doi.org/10.1016/j.compstruct.2014.11.003.

[7] Duarte I, Vesenjak M, Krstulović-Opara L, Ren Z. Compressive performance evaluation of APM (Advanced Pore Morphology) foam filled tubes. Compos Struct 2015;134:409–20. https://doi.org/10.1016/j.compstruct.2015.08.097.

[8] Duarte I, Vesenjak M, Krstulović-Opara L, Ren Z. Static and dynamic axial crush performance of in-situ foam-filled tubes. Compos Struct 2015;124:128–39. https://doi.org/10.1016/j.compstruct.2015.01.014.

[9] Duarte I, Krstulović-Opara L, Vesenjak M. Axial crush behaviour of the aluminium alloy in-situ foam filled tubes with very low wall thickness. Compos Struct 2018;192:184–92. https://doi.org/10.1016/j.compstruct.2018.02.094.

[10] Fang J, Gao Y, An X, Sun G, Chen J, Li Q. Design of transversely-graded foam and wall thickness structures for crashworthiness criteria. Compos Part B Eng 2016;92:338–49. https://doi.org/10.1016/j.compositesb.2016.02.006.

[11] Wang Y, Liew JYR, Lee SC, Zhai X, Wang W. Crushing of a novel energy absorption connector with curved plate and aluminum foam as energy absorber. Thin-Walled Struct 2017;111:145–54. https://doi.org/10.1016/j.tws.2016.11.019.

[12] Wang Y, Zhai X, Ying W, Wang W. Dynamic crushing response of an energy absorption connector with curved plate and aluminum foam as energy absorber. Int J Impact Eng 2018;121:119–33. https://doi.org/10.1016/j.ijimpeng.2018.07.016.

[13] Burlayenko VN, Sadowski T. Effective elastic properties of foam-filled honeycomb cores of sandwich panels. Compos Struct 2010;92:2890–900. https://doi.org/10.1016/j.compstruct.2010.04.015.

[14] Liu J, Chen W, Hao H, Wang Z. Numerical study of low-speed impact response of sandwich panel with tube filled honeycomb core. Compos Struct 2019;220:736–48. https://doi.org/10.1016/j.compstruct.2019.04.023.

[15] Evans KE, Nkansah MA, Hutchinson IJ, Rogers SC. Molecular Network Design. Nature 1991;353:124. https://doi.org/10.1038/353124a0.

[16] Grima JN, Gatt R, Ravirala N, Alderson A, Evans KE. Negative Poisson's ratios in cellular foam materials. Mater Sci Eng A 2006;423:214–8. https://doi.org/10.1016/j.msea.2005.08.229.

[17] Hou S, Liu T, Zhang Z, Han X, Li Q. How does negative Poisson's ratio of foam filler affect crashworthiness? Mater Des 2015;82:247–59.

https://doi.org/10.1016/j.matdes.2015.05.050.

[18] Novak N, Vesenjak M, Ren Z. Auxetic cellular materials - a Review. Strojniški Vestn - J Mech Eng 2016;62:485–93. https://doi.org/10.5545/sv-jme.2016.3656.

[19] Wu W, Hu W, Qian G, Liao H, Xu X, Berto F. Mechanical design and multifunctional applications of chiral mechanical metamaterials: A review. Mater Des 2019;180:107950. https://doi.org/10.1016/J.MATDES.2019.107950.

[20] Ma C, Lei H, Liang J, Wu W, Wang T, Fang D. Macroscopic mechanical response of chiral-type cylindrical metastructures under axial compression loading. Mater Des 2018;158:198–212. https://doi.org/10.1016/J.MATDES.2018.08.022.

[21] Lu Q, Qi D, Li Y, Xiao D, Wu W. Impact energy absorption performances of ordinary and hierarchical chiral structures. Thin-Walled Struct 2019;140:495–505. https://doi.org/10.1016/J.TWS.2019.04.008.

[22] Xiao D, Chen X, Li Y, Wu W, Fang D. The structure response of sandwich beams with metallic auxetic honeycomb cores under localized impulsive loading-experiments and finite element analysis. Mater Des 2019;176:107840. https://doi.org/10.1016/J.MATDES.2019.107840.

[23] Novak N, Vesenjak M, Krstulović-Opara L, Ren Z. Mechanical characterisation of auxetic cellular structures built from inverted tetrapods. Compos Struct 2018;196:96–107. https://doi.org/10.1016/j.compstruct.2018.05.024.

[24] Duncan O, Foster L, Senior T, Alderson A, Allen T. Quasi-static characterisation and impact testing of auxetic foam for sports safety applications. Smart Mater Struct 2016;25:054014. https://doi.org/10.1088/0964-1726/25/5/054014.

[25] Xiao D, Dong Z, Li Y, Wu W, Fang D. Compression behavior of the graded metallic auxetic reentrant honeycomb: Experiment and finite element analysis. Mater Sci Eng A 2019;758:163–71. https://doi.org/10.1016/j.msea.2019.04.116.

[26] Xue Y, Wang X, Wang W, Zhong X, Han F. Compressive property of Al-based auxetic lattice structures fabricated by 3-D printing combined with investment casting. Mater Sci Eng A 2018;722:255–62. https://doi.org/10.1016/j.msea.2018.02.105.

[27] Novak N, Hokamoto K, Vesenjak M, Ren Z. Mechanical behaviour of auxetic cellular structures built from inverted tetrapods at high strain rates. Int J Impact Eng 2018;122:83–90. https://doi.org/https://doi.org/10.1016/j.ijimpeng.2018.08.001.

[28] Qiao JX, Chen CQ. Impact resistance of uniform and functionally graded auxetic double arrowhead honeycombs. Int J Impact Eng 2015;83:47–58. https://doi.org/10.1016/j.ijimpeng.2015.04.005.

[29] Jin X, Wang Z, Ning J, Xiao G, Liu E, Shu X. Dynamic response of sandwich structures with graded auxetic honeycomb cores under blast loading. Compos Part B Eng 2016;106:206–17. https://doi.org/10.1016/j.compositesb.2016.09.037.

[30] Hou X, Deng Z, Zhang K. Dynamic Crushing Strength Analysis of Auxetic

Honeycombs. Acta Mech Solida Sin 2016;29:490–501. https://doi.org/10.1016/S0894-9166(16)30267-1.

[31] Huang J, Zhang Q, Scarpa F, Liu Y, Leng J. In-plane elasticity of a novel auxetic honeycomb design. Compos Part B Eng 2017;110:72–82. https://doi.org/10.1016/j.compositesb.2016.11.011.

[32] Imbalzano G, Linforth S, Ngo TD, Lee PVS, Tran P. Blast Resistance of Auxetic and Honeycomb Sandwich Panels: Comparisons and Parametric Designs. Compos Struct 2017;183:242–61. https://doi.org/10.1016/j.compstruct.2017.03.018.

[33] Novak N, Starčevič L, Vesenjak M, Ren Z. Blast response study of the sandwich composite panels with 3D chiral auxetic core. Compos Struct 2019;210:167–78. https://doi.org/https://doi.org/10.1016/j.compstruct.2018.11.050.

[34] Mohsenizadeh S, Alipour R, Shokri Rad M, Farokhi Nejad A, Ahmad Z. Crashworthiness assessment of auxetic foam-filled tube under quasi-static axial loading. Mater Des 2015;88:258–68. https://doi.org/10.1016/j.matdes.2015.08.152.

[35] Mohsenizadeh S, Ahmad Z. Auxeticity effect on crushing characteristics of auxetic foam-filled square tubes under axial loading. Thin-Walled Struct 2019;145:106379. https://doi.org/10.1016/j.tws.2019.106379.

[36] Jiang L, Hu H. Low-velocity impact response of multilayer orthogonal structural composite with auxetic effect. Compos Struct 2016. https://doi.org/10.1016/j.compstruct.2016.10.018.

[37] Smardzewski J, Jasińska D, Janus-Michalska M. Structure and properties of composite seat with auxetic springs. Compos Struct 2014;113:354–61. https://doi.org/10.1016/j.compstruct.2014.03.041.

[38] Alderson A, Alderson KL, Attard D, Evans KE, Gatt R, Grima JN, et al. Elastic constants of 3-, 4- and 6-connected chiral and anti-chiral honeycombs subject to uniaxial in-plane loading. Compos Sci Technol 2010;70:1042–8. https://doi.org/10.1016/j.compscitech.2009.07.009.

[39] Prall D, Lakes RS. Properties of a chiral honeycomb with a poisson's ratio of — 1. Int J Mech Sci 1997;39:305–14. https://doi.org/10.1016/S0020-7403(96)00025-2.

[40] Corp DSS. Abaqus Theory Guide. Warwick, RI, USA: Dassault Systémes Simulia Corp; 2013. https://doi.org/10.1017/CBO9781107415324.004.

[41] Ghamarian A, Tahaye Abadi M. Axial crushing analysis of end-capped circular tubes. Thin-Walled Struct 2011;49:743–52. https://doi.org/10.1016/j.tws.2011.01.006.

[42] Körner C. Additive manufacturing of metallic components by selective electron beam melting — a review. Int Mater Rev 2016;61:361–77. https://doi.org/10.1080/09506608.2016.1176289.

[43] Heinl P, Körner C, Singer RF. Selective electron beam melting of cellular titanium: Mechanical properties. Adv Eng Mater 2008;10:882–8.

https://doi.org/10.1002/adem.200800137.

[44] Borovinšek M. OptiMax - Online Users Manual n.d. http://lace.fs.uni-mb.si/wordpress/borovinsek/?page_id=104 (accessed December 22, 2019).